PLDI-Based Convexification for Roll-to-Roll Dry Transfer Control

C. Martin*, Q. Zhao **, S. Bakshi *, D. Chen****, W. Li*****

The University of Texas at Austin, Austin, TX, 78712, USA
*(e-mail: cbmartin129@utexas.edu), **(e-mail: qishenzhao0904@utexas.edu), ***(e-mail: soovadeep.bakshi@utexas.edu), ****(e-mail: dmchen@me.utexas.edu), *****(e-mail: weiwli@austin.utexas.edu)

Abstract: Roll-to-Roll **(**R2R) mechanical peeling for dry transfer has the potential to enable high throughput production of 2D materials and flexible electronics, while minimizing the environmental impact. The dry transfer process is highly nonlinear, involving challenging peeling front dynamics. In this study, a novel convexification scheme is developed based on polytopic linear differential inclusions (PLDI). An LQR controller is used to establish that the performance of a linear approximation built using this PLDI-based method is consistently superior to that of a Taylor's expansion-based approximation, demonstrating that the PLDI-based scheme is an effective control tool for complex systems, including the R2R mechanical peeling process.

Keywords: Roll-to-Roll (R2R), Peeling Front, 2D Materials Dry Transfer, PLDI, Convexification, Printed Electronics.

1. INTRODUCTION

In the realm of flexible electronics, transfer printing is a class of methods that retrieve printed electronic features from a printed substrate and move them to a target substrate to build more advanced flexible electronic devices (Linghu et al., 2018). Improving this transfer process is critical to the development of multi-layered microelectronic devices (Zhou et al., 2019). Until now, research has focused on device printing rather than transferring (Khan et al., 2020). For 2D materials such as electronic-grade graphene, the typical manufacturing process involves growing these materials on a substrate and then dissolving that substrate in acid. This dissolution process causes environmental concerns and the loss of the substrate material. To address these issues, Sun et al. (2016), proposed a method where an electrochemical bubbling method was used to separate the 2D material from the growth substrate; however, the energy release by bubble collapse could damage the transferred material. As an alternative, a roll-to-roll (R2R) dry transfer process was developed by Xin et al. (2018). The process has the potential to minimize chemical waste and other adverse environmental effects. Most importantly, it can be used to significantly increase the throughput of 2D materials manufacturing.

The R2R dry transfer process involves mechanical peeling of printed patterns or thin films, such as graphene made using chemical vapor deposition (CVD), from a substrate and depositing it onto another in a continuous manner. Controlling the web tension has been identified as one of the critical objectives of the peeling process (Zhao et al., 2020). Previous work has demonstrated that R2R mechanical peeling is a viable method for high-throughput production of CVD graphene. However, the process precision needs to further improve to produce microelectronic-grade graphene for device fabrication. In addition to graphene, the R2R dry transfer process has the potential to enable high-throughput production of sophisticated flexible electronic devices through transfer printing. Currently, there does not exist a R2R transfer process for printed micro-electronic devices.

Controlling such a R2R mechanical peeling process is challenging since the process is highly nonlinear due to variations in the adhesion energy between the material-to-transfer and the substrate, the viscoelastic nature of the flexible substrates, and the fact that the web tension and speed control are coupled. Researchers have used nonlinear optimization techniques to control the tension and speed of R2R processes, but none of them involved mechanical peeling (Jabbar and Pagilla, 2016; Chen et al., 2018). Zhao, et al., (2020) developed a linear model of the R2R peeling front by assuming that the peeling front velocity was constant. A nonlinear model was subsequently developed to account for the varying peeling front velocity (Zhao, et al., 2021) and is adapted in this work to develop a polytopic linear differential inclusion (PLDI)-based convexification strategy for the R2R peeling process.

Previously, PLDI methods have been used for robust control design by constraining the worst-case error of a linearized system such that the developed controller can achieve guaranteed stability or optimality properties (Olalla et al., 2009; Tanaka, 1996). This paper takes a new and further step by exploring the use of terms produced by the PLDI method for system convexification, such that a more accurate linear representation can be obtained. Rodrigues et al. (2011) and Kuiava et al. (2012) used a similar PLDI-based convexification method, but their method is only valid for control-affine systems and cannot be applied to the R2R peeling process. The PLDI-based convexification strategy developed in this paper is valid for all nonlinear systems and can be applied to the R2R peeling process. The convexification approach used in this paper is chosen instead of other convexification methods, such as the Koopman operator method (Mezić, 2015; Korda and Mezić, 2018), because the PLDI-based method is reversible, meaning one can maintain a connection between the linear approximation and the

nonlinear terms of the system model to facilitate control design and enable a tradeoff analysis between process development and control optimization. In contrast, the Koopman operator lifts the nonlinear system into a high dimensional space in such a way that the link to the variables in the nonlinear space is lost. This reversibility property of the PLDI convexification method, along with the fact that the convex matrix set that bounds the linear approximation changes with the system state, suggest that this convexification strategy could be amenable to the control design, for instance, of model predictive control (MPC) controllers in future work.

In this paper, a nonlinear model is presented to describe the R2R peeling process. A PLDI-based scheme is used to perform the convexification, based on which an LQR control problem is formulated. This control method is then applied to the nonlinear peeling system, and the overall system performance is contrasted with that of a conventional method using averaged Taylor approximation. It is shown that the proposed PLDI-based convexification method is far superior to classical methods in linear approximations.

2. THE NONLINEAR R2R PEELING SYSTEM MODEL

Figure 1 shows a schematic of the R2R process (Zhao, et al, 2021). The unwinding roller supplies a laminated roll of donor and receiver substrates, and a pair of nipping rollers are used to peel the laminate. After peeling, the two rewinding rollers collect the two substrates. The peeling front is shown in Fig. 2. Roller 1 is the unwinding roller and rollers 2 and 3 are the rewinding rollers. v_1, v_2, and v_3 represent the linear velocities of the web on the three rollers. D_1, D_2, and D_3 represent the distance along the web from each of the three rollers to the nipping rollers. Let C_1 be the web section from the unwinding roller to the peeling front, while C_2 and C_3 be the two web sections that stretch between the two rewinding rollers and the peeling front. ε_1, ε_2, and ε_3 represent the strains of three web sections. θ_1 and θ_2 are the angles between a line extending from C_1 at the peeling front and C_3 and C_2, respectively. β and γ are the angles correspond to the contact sections of C_1 and C_3 when they wrap around corresponding nipping rollers. h is the distance along C_3 from the peeling front to the nipping roller. R is the radius of the nipping rollers.

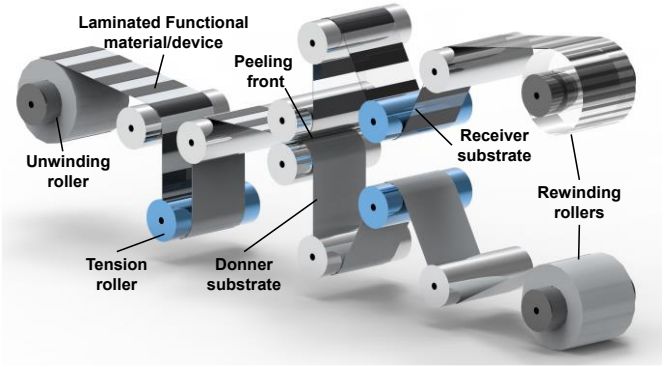

Fig. 1. The R2R peeling process: Overall R2R schematic (Zhao, et al, 2021)

The nonlinear R2R peeling model is summarized as follows (Zhao, et al., 2021). First, the relationship between the web tensions t_1, t_2, and t_3 and the peeling front geometry can be expressed as

$$t_1 = t_3 \cos\theta_1 + t_2 cos\theta_2 \tag{1}$$

$$t_3 sin\theta_1 = t_2 sin\theta_2. \tag{2}$$

With v_1 constant, the time derivatives of v_2 and v_3 can be defined as

$$\dot{v}_i(t) = -\frac{R_i^2}{J_i} t_i(t) + \frac{R_i}{J_i} u_i(t) - \frac{f_i}{R_i} v_i(t), i = 2,3 \tag{3}$$

where R_i is the radius, J_i is the moment of inertia, and f_i is the damping coefficient of the corresponding rewinding roller.

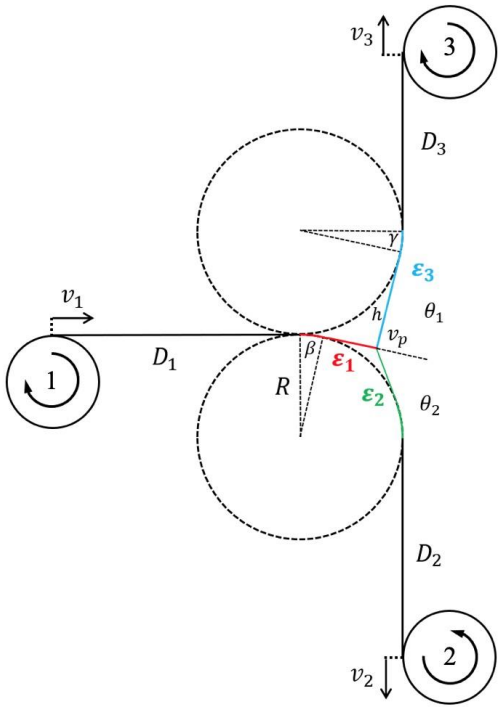

Fig. 2. Peeling Front: A detailed look at the R2R peeling front (Zhao, et al, 2021)

If l_1, l_2, and l_3 are defined as the unstretched lengths of the webs corresponding to the three web sections and L_1, L_2, and L_3 are the actual length of the web sections, then

$$l_i(t) = \frac{L_i(t)}{1+\varepsilon_i(t)}, i = 1,2,3 \tag{4}$$

$$\dot{l_1}(t) = \frac{v_1(t) - v_p(t)}{1+\varepsilon_1(t)} \tag{5}$$

$$\dot{l_2}(t) = \frac{v_p(t)}{1+\varepsilon_1(t)} - \frac{v_2(t)}{1+\varepsilon_2(t)} \tag{6}$$

$$\dot{l_3}(t) = \frac{v_p(t)}{1+\varepsilon_1(t)} - \frac{v_3(t)}{1+\varepsilon_3(t)} \tag{7}$$

where v_p is the peeling front velocity, defined as the speed of separation of the webs as observed from C_1. The complex plane method can be used to define the following equations.

$$\frac{R}{cos(\theta_2/2)} \cdot e^{i\cdot\left(\frac{\pi-\theta_2(t)}{2}-\beta(t)\right)} + h(t) \cdot e^{i\cdot(\theta_1(t)-\beta(t))} - R \cdot e^{i\cdot(-\gamma(t))} = 2R \cdot e^{i\cdot\frac{\pi}{2}} \quad (8)$$

$$\beta(t) - \gamma(t) + \frac{\pi}{2} = \theta_1(t) \quad (9)$$

$$L_1(t) - D_1 = R \cdot \beta(t) + R \cdot tan\left(\frac{\theta_2(t)}{2}\right) \quad (10)$$

$$L_2(t) - D_2 = R \cdot \left\{\frac{\pi}{2} - \beta(t) - \theta_2(t) + tan\left(\frac{\theta_2(t)}{2}\right)\right\} \quad (11)$$

$$L_3(t) - D_3 = R \cdot \gamma(t) + h(t) \quad (12)$$

Finally, the peeling front velocity, v_p, depends on the relationship between the mechanical energy release rate, G, and the adhesion energy between the laminate and the substrate, Γ. G can be found using the following equation,

$$G = \frac{t_3}{b}(1 - cos\theta_1 + \varepsilon_3 - \varepsilon_1) + \frac{t_2}{b}(1 - cos\theta_2 + \varepsilon_2 - \varepsilon_1) - \frac{h_{w3}\cdot E_3}{2(1+\varepsilon_1)}(\varepsilon_3^2 - \varepsilon_1^2) - \frac{h_{w2}\cdot E_2}{2(1+\varepsilon_1)}(\varepsilon_2^2 - \varepsilon_1^2) \quad (13)$$

where b is the web width, and h_{w2} and h_{w3} are the thicknesses of C_2 and C_3, respectively. When $\Gamma > G$, peeling cannot occur, so $v_p = 0$. When $\Gamma = G$, peeling occurs, so v_p will be a positive value. Due to physical constraints, G cannot be greater than Γ.

Unlike the previous work (Zhao, et al., 2021), where a discrete time method is applied to model the system using the constraint that $\Gamma \geq G$, a continuous time nonlinear approach is employed to represent the system in the following state-space form,

$$\dot{x} = f(x,u),\ x = [v_2, v_3, t_1, t_2, t_3]^T,\ u = [u_2, u_3]^T \quad (14)$$

where u_2 and u_3 are torque inputs on the two rewinding rollers. This state space form is desirable because it can be readily applied to control design. To represent the system in this form, one must define v_p in a continuous, differentiable fashion, and v_p must be a function of the system states. A novel approach is proposed in this study to represent v_p in this manner.

To approximate v_p, a heuristic approach is taken, where the discrete time method is used to find v_p as a function of G-Γ with v_2 and v_3 held constant, and v_p as a function of the average of v_2 and v_3, with G-Γ held constant. According to this approximation, v_p varies logarithmically with G-Γ and linearly with the average of v_2 and v_3. In addition, at steady-state, when $G = \Gamma$,

$$v_p = v_2 = v_3 = v_1 \quad (15)$$

where v_1 is the constant unwinding velocity. A piece-wise continuous, differentiable function that follows the two heuristics and (15) is,

$$v_p = \begin{cases} \frac{v_2+v_3}{2} \cdot \left(1 + ln\left(1 + (G - \Gamma)\right)\right), & G - \Gamma > -1 \\ 0, & G - \Gamma \leq -1 \end{cases} \quad (16)$$

where there is a lower saturation limit at zero, as v_p cannot be negative.

This functional approximation of v_p has all the stated desirable properties: it represents v_p as a function of state variables, and it is continuous and differentiable in the neighbourhood of the stable operating point $G = \Gamma$. It also aligns well with the trends of the discontinuous model. Thus, (16) represents a novel and reasonable approximation of v_p that characterizes the peeling front in a state space form.

Next, the three tensions as a function of the three unstretched lengths can be found using (1), (2), (4), and (8)-(12). It should be noted that their relationship cannot be determined analytically. To find a solution, an iterative approach was used to generate three interpolation maps, one for each tension value. These maps were used to estimate the partial derivatives of each tension value with respect to each of the three unstretched lengths. Using this strategy, the following equation defines the tension time derivatives,

$$\dot{t_i} = \frac{\partial t_i}{\partial l_1}(\mathrm{t}) \cdot \dot{l_1} + \frac{\partial t_i}{\partial l_2}(\mathrm{t}) \cdot \dot{l_2} + \frac{\partial t_i}{\partial l_3}(\mathrm{t}) \cdot \dot{l_3},\ i = 1,2,3 \quad (17)$$

where the partial derivatives are defined numerically, as described above, and (5)-(7) define the three unstretched length derivatives. Thus, (3) and (17) define the state derivatives of the R2R system as a function of states and inputs to allow the system representation in the form of (14).

3. THE PLDI-BASED CONVEXIFICATION STRATEGY

This section presents a novel method to create a linear estimation of the system to facilitate control design. A PLDI convexification approach similar to the one used in Rodrigues et al., (2011) is applied. A nonlinear system in a state space form, such as (14), can be transformed into

$$f(x,u) = f(y) = [f_1(y), f_2(y), \dots, f_n(y)]^T \quad (18)$$

where $y = [x,u]^T, x \in \mathbb{R}^n, u \in \mathbb{R}^m$, $q = n + m$, *and* $f_i: \mathbb{R}^q \rightarrow \mathbb{R}$. Using this representation, *f(y)* can be rewritten as

$$f(y) = \sum_{i=1}^{n} V_n(i) f_i(y)\,, V_n(i) = [0, 0, \dots, 1^i, \dots, 0\,]^T \quad (19)$$

Next, the mean value theorem for multi-dimensional functions states that

$$Let\ f(y): \mathbb{R}^q \rightarrow \mathbb{R}^n; \mu, \rho \in \mathbb{R}^q;\ \exists\ \sigma_1, \sigma_2, \dots, \sigma_n\ such\ that,$$

$$f(\mu) - f(\rho) = \left(\sum_{i=1}^{n}\sum_{j=1}^{q} V_{ij}\frac{\partial f_i(\sigma_i)}{\partial y_j}\right)(\mu - \rho) \quad (20)$$

where $V_{ij} = V_n(i)V_q^T(j)$, and $\sigma_1, \sigma_2, \dots, \sigma_n$ are in the convex hull of μ and ρ.

Based on (18)-(20), a PLDI-based convexification strategy is proposed as follows. At each equilibrium operating point, the following method is used to approximate an upper and lower bound of the true state and control matrix A_y. First, define vectors $\overline{v}_1, \underline{v}_1, \overline{v}_2, \underline{v}_2, \dots \overline{v}_n, \underline{v}_n \in Co\big(y(t), \hat{y}(t)\big)$, where *Co(·)* denotes the convex hull, such that

$$\frac{\partial f_i}{\partial y}(\overline{v}_i) \cdot (y - \hat{y}) = \max_{y_{si}}\left\{\frac{\partial f_i}{\partial y}(y_{si}) \cdot (y - \hat{y})\right\} \quad (21)$$

$$\frac{\partial f_i}{\partial y}\left(\underline{v}_i\right) \cdot (y - \hat{y}) = \min_{y_{si}}\left\{\frac{\partial f_i}{\partial y}(y_{si}) \cdot (y - \hat{y})\right\} \quad (22)$$

can be found, where $\hat{y}(t)$ is a stable operating point, *y(t)* is some trajectory near, but not the same as, $\hat{y}$, and $y_{si}(t) \in Co\big(y(t), \hat{y}(t)\big)$. Thus, finding the $\overline{v}_i, \underline{v}_i$ values involves maximizing and minimizing the function $\frac{\partial f_i}{\partial y}(y_{si}) \cdot (y - \hat{y})$ along the line $Co\big(y(t), \hat{y}(t)\big)$ in q-dimensional space. This optimization problem could be challenging in general, but for the function *f* and the vector $y = [x, u]^T$ defined in (14), the function $\frac{\partial f_i}{\partial y}(y_{si}) \cdot (y - \hat{y})$ is continuous and differentiable, so for the application discussed in this paper the optimization problems (21) and (22) are straightforward. Once the $\overline{v}_i, \underline{v}_i$ values are found, by (20), and observing that $\dot{\hat{x}} = 0$, the state derivatives can be bounded in the following manner,

$$\dot{x} \in \left(Co\left\{\sum_{i=1}^{n}\sum_{j=1}^{q} V_{ij}\delta_{ij}\right\}\right)(y - \hat{y}) \tag{23}$$

where $\delta_{ij} \in \left\{\frac{\partial f_i}{\partial y_j}(\overline{v}_i), \frac{\partial f_i}{\partial y_j}\left(\underline{v}_i\right)\right\}$. Using this representation, one can define a convex PLDI Ω_{PLDI}, as presented in Boyd et al. (1994), whose trajectories contain all possible solutions to (23), by the set of vertices,

$$V_{PLDI} = \left\{\sum_{i=1}^{n}\sum_{j=1}^{q} V_{ij}\delta_{ij} \,:\, \delta_{ij} \in \left\{\frac{\partial f_i}{\partial y_j}(\overline{v}_i), \frac{\partial f_i}{\partial y_j}\left(\underline{v}_i\right)\right\}\right\}. \tag{24}$$

In the proposed convexification scheme, the scope of possible system matrices is further restricted to be within the set

$$A_{PLDI} \in \left\{\overline{A_{PLDI}} \cdot \lambda + \underline{A_{PLDI}} \cdot (1 - \lambda) \,:\, \lambda \in [0,1]\right\} \tag{25}$$

where A_{PLDI} is an estimation of the true system matrix A_y, λ is a weighting factor that represents a tradeoff between the lower and upper bounds, and

$$\overline{A_{PLDI}} = \sum_{i=1}^{n}\sum_{j=1}^{q} V_{ij}\frac{\partial f_i}{\partial y_j}(\overline{v_i}) \tag{26}$$

$$\underline{A_{PLDI}} = \sum_{i=1}^{n}\sum_{j=1}^{q} V_{ij}\frac{\partial f_i}{\partial y_j}\left(\underline{v_i}\right). \tag{27}$$

Thus, an estimation is made on the true system matrix A_y that is a bounded, convex combination of two matrices $\overline{A_{PLDI}}, \underline{A_{PLDI}} \in V_{PLDI}$.

To demonstrate that the proposed PLDI convexification scheme can be used for control design and to compare its effectiveness to that of Taylor's expansion, an LQR controller was developed. Using (25), a linear representation of the system as defined by (14) was developed. Then, using an averaged Taylor's method, another linear representation of the same system was developed. The LQR problem was then solved using each of these two system matrix approximations to obtain K_{PLDI} and K_{Taylor}. The system control law was chosen to be

$$u = -K \cdot x, \tag{28}$$

where *K* was K_{PLDI} or K_{Taylor}, and *x* and *u* are the same as those in (14). For each run, the *Q* and *R* matrices were changed in the LQR problem to optimize the performance at that specific equilibrium operating point $\hat{y}$. These two gain matrices were used to control the nonlinear model developed in Section 2 to follow a reference trajectory that moved in steps around $\hat{y}$. The K_{PLDI} gain matrix consistently resulted in superior control performance to the K_{Taylor} matrix. This convexification and control scheme was performed around 5 different stable operating points of $\hat{y}$.

4. RESULTS AND DISCUSSION

4.1 Model Validation

Experimental data was used to validate the differentiable representation of v_p developed in this study. The experiments were conducted by peeling apart two polyethylene terephthalate (PET) films heat sealed together using a hot roll laminator. Note that, during the peeling, the t_2 reference, t_3 reference, and v_1 values were held constant. The experiments consisted of six different runs with different combinations of constant t_2 reference, t_3 reference, and v_1 values. The average θ_1 and θ_2 values for each of the six runs were measured and Γ was determined based on the model.

Simulations were performed using the model presented in Section 2 at the same set points as those in the experiments. Table 1 presents the simulation and experimental results. The first three columns show the set points for the t_2 reference, t_3 reference, and Γ values that were used in the experiments and simulations; the next four columns show the average θ_1 and θ_2 values for the six parallel experiments and simulations, respectively; and the final column shows the percent difference between these average θ_1 and θ_2 results for each experiment-simulation pair. In both the experiments and the simulations, neither θ_1 nor θ_2 was controlled directly, so agreement between the θ_1 and θ_2 values in the experiments and simulations would validate the model.

Table 1. Steady state model validation

t_2 Ref. (N)	t_3 Ref. (N)	Γ Ref. (J/m^2)	θ_1 Exp.	θ_1 Sim.	θ_2 Exp.	θ_2 Sim.	Absolute Diff. (%)	
							θ_1	θ_2
9.9	20.0	149.3	28.8°	28.4°	103.6°	105.3°	1.4	1.6
10.0	15.7	154.5	40.6°	38.4°	103.5°	101.6°	5.4	1.8
9.8	20.0	137.4	29.1°	28.6°	96.8°	99.4°	1.7	2.7
15.5	19.6	172.1	48.2°	48.4°	71.0°	71.3°	0.4	0.4
15.0	19.8	161.5	45.5°	45.6°	70.2°	70.8°	0.2	0.9
19.9	20.2	204.6	59.5°	59.8°	61.1°	61.3°	0.5	0.3

Notice that in all cases the absolute percent difference between the simulation and experimental average θ_1 and θ_2 data is less than 6%, and in all cases but one the percent difference is less than 3%. This suggests that the model can describe the steady state operation of the peeling process with high accuracy.

The next experimental validation set investigates the system transient response under a step tension input. In this experiment the t_2 and t_3 reference values underwent a step change from 26.5 N and 27 N, to 28 N and 34 N, and back to 26.5 N and 27 N, respectively. In addition, Γ varied from an average of 260 J/m^2 at the first tension state to an average of

230 J/m^2 at the second state, and then back to 260 J/m^2. The adhesion energy Γ varies stochastically with time, and this is important in the transient case because the variation causes dynamics at the peeling front. In contrast to other continuous time modelling techniques, the proposed model can represent these random peeling front dynamics accurately because it represents v_p as a function of Γ.

A simulation was conducted that tracked the same tension reference trajectory as the experiment did. To simulate its stochastic nature, Γ was set to follow the same average trajectory as in the experimental case, but with added Gaussian noise with a variance of 10 (J/m^2)^2. Figure 3 presents the experimental and simulation data. Figure 3(a) shows the simulation step response data. Figure 3(b) shows the experimental step response data. The figure also shows the θ_1 and θ_2 values from both the simulation (Fig. 3(c)) and the experiment (Fig. 3(d)). Note that both the testing and simulated systems tracked the reference tension trajectories well, and that the t_1 values of the simulation matched those of the experiment. In addition, the simulated and experimental peeling angles follow the same trajectories, disregarding the noise.

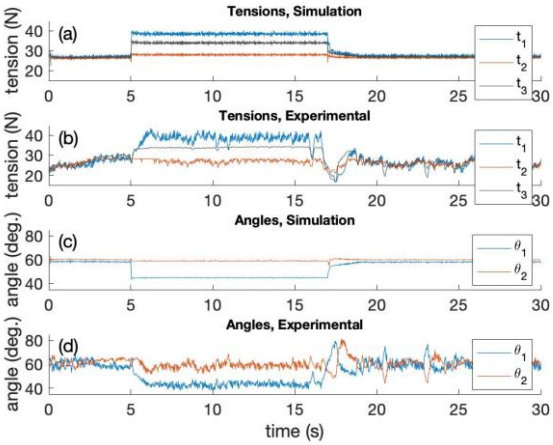

Fig. 3. Step-response model validation

4.2 Simulation Results of Convex PLDI-Based Control

After validation of the differentiable representation of v_p, an LQR control framework was used to compare the web tension control performance of the proposed convex PLDI-based scheme to that of the Taylor's expansion method. This study focuses on web tension control because controlling the web tensions is equivalent to controlling the peeling angle, and past work has demonstrated that controlling the peeling angle is critical to the R2R dry transfer process (Zhao et al., 2020).

Figure 4 shows the t_3 results in one of the five simulated runs, each around a different stable operating point. In Fig. 4, the graph on the top shows the LQR-controlled system response using the convex PLDI-based scheme as defined by (25), while the graph at the bottom shows the LQR-controlled system response using the Taylor's expansion scheme. The system t_3 response is in red, while the reference t_3 trajectory is in blue. The inserts of both graphs show zoomed the part of the run with the largest overshoot. The system response shown in Fig. 4 is similar to that of the other runs.

Notice that both linear models resulted in control schemes that performed well. The settling time was about the same for both methods, but the overshoot was much less in the graph corresponding to the convex PLDI-based linear model. This difference is significant, as overshoot is the critical control parameter for the R2R peeling process. Excessive overshoot will cause defects in the transfer of graphene or printed electronics. Thus, Fig. 4 suggests that the convex PLDI-based method can improve the performance of the R2R peeling.

Table 2 summarizes the tension overshoots for both the PLDI-based and Taylor-based controls on the five runs around different equilibrium points. Each of the four columns under the headings "PLDI Average Overshoot" and "Taylor's Approx. Average Overshoot" contain the mean t_2 and t_3 overshoots for each of the steps in each of the simulated runs, all of which are similar to those that have been shown in Fig. 4. The tensions under the "PLDI Average Overshoot" heading correspond to the runs that were controlled using the convex PLDI-based scheme, while the tensions under the "Taylor's Approx. Average Overshoot" heading correspond to the Taylor's approximation-based control. The final two columns contain the percent difference between the average t_2 and t_3 overshoots, respectively, corresponding to the two methods at each operating point.

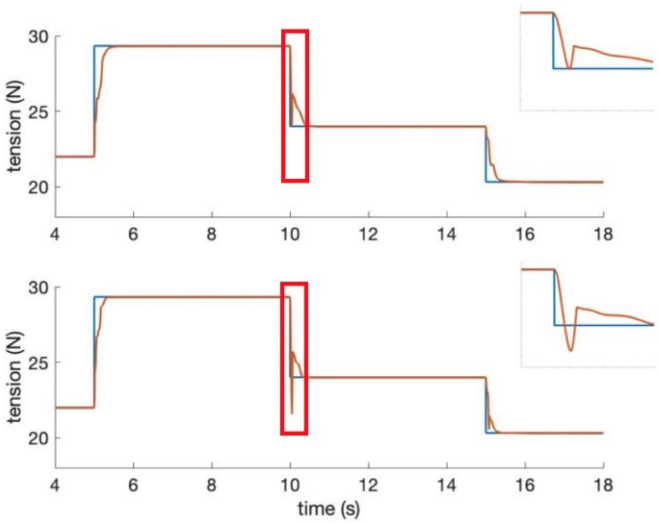

Fig. 4. Simulated LQR control based on both linear approximations

Table 2. Overshoot Comparison

Run #	PLDI Average Overshoot		Taylor's Approx. Average Overshoot		t_2 Percent Diff. (%)	t_3 Percent Diff. (%)
	t_2 (N)	t_3 (N)	t_2 (N)	t_3 (N)		
1	1.90E-3	2.51E-1	8.13E-3	5.13E-1	76.6	51.1
2	0.00E+0	1.53E-1	0.00E+0	2.66E-1	N/A	42.5
3	8.72E-1	1.10E+0	9.71E-1	1.21E+0	10.1	8.9
4	4.20E-1	5.74E-1	8.09E-1	1.27E+0	48.1	54.6
5	6.41E-1	5.64E-1	7.37E-1	7.81E-1	13.0	27.9

The results in Table 2 show that the transient performance of the convex PLDI-based scheme outperformed the that of the Taylor expansion-based scheme by 10-70% in overshoot. These results suggest that the novel convex PLDI-based scheme can significantly improve the peeling angle control performance of the R2R peeling process. Thus, the PLDI-based method can be an enabling tool that will allow high quality R2R dry transfer of CVD graphene and printed electronics.

5. CONCLUSIONS

This paper presented a nonlinear, continuous time adaptation of a discrete model for a R2R mechanical peeling system and developed a methodology for convexifying nonlinear systems using a PLDI approach. The continuous time adaptation contains a novel way to represent the peeling front velocity as a continuous and differentiable function, and this approach was experimentally validated. An LQR control platform was established to compare the benefits of the proposed convex PLDI-based modeling to that of the conventional Taylor's expansion. The simulation results showed that the PLDI-based approach resulted in 10-70% less tension overshoot than Taylor's expansion. This improvement suggests that the PLDI-based convexification scheme will be able to significantly improve the dry transfer quality of 2D materials and printed electronics in a R2R process. In addition, the improved accuracy is critical for other high precision manufacturing processes, such as the R2R manufacturing of electrode assembly for lithium-ion batteries, proton exchange membrane fuel cells, and organic solar cells.

ACKNOWLEDGMENT

This material is based upon work supported by the National Science Foundation under Grant No. 2041470. Any opinions, findings and conclusions or recommendations expressed in this material are those of the author(s) and do not necessarily reflect the views of the National Science Foundation.

REFERENCES

Boyd, S., El Ghaoui, L., Feron, E., and Balakrishnan, V. (1994). *Linear matrix inequalities in system and control theory*. Siam.

Chen, W.-T., Chowdhury, R. A., Youngblood, J., and Chiu, G. T.-C. (2018). A Two-step Thresholding Algorithm for Image-based Defect Detection in Roll-to-Roll Coating of Cellulose Nanocrystal Films. *2018 Annual American Control Conference (ACC)*, IEEE, pp. 4440-4445.

Jabbar, K. A. and Pagilla, P. R. (2016). Optimal velocity profile design for transport of viscoelastic webs in roll-to-roll manufacturing. *2016 American Control Conference (ACC)*, IEEE, pp. 1729-1734.

Khan, Y., Thielens, A., Muin, S., Ting, J., Baumbauer, C., and Arias, A. C. (2020). A New Frontier of Printed Electronics: Flexible Hybrid Electronics. *Advanced Materials,* vol 32, no. 15, p. 1905279.

Korda, M. and Mezić, I. (2018). Linear predictors for nonlinear dynamical systems: Koopman operator meets model predictive control. *Automatica*, vol. 93, pp. 149-160.

Kuiava, R., Ramos, R. and Pota, H. (2012). A new approach for modeling and control of nonlinear systems via norm-bounded linear differential inclusions. *Sba: Controle & Automação Sociedade Brasileira de Automatica*, 23(4), pp.387-403.

Linghu, C., Zhang, S., Wang, C., and Song, J. (2018). Transfer printing techniques for flexible and stretchable inorganic electronics. *npj Flexible Electronics,* vol. 2, no. 1, p. 26,

Mezić, I. (2015). On applications of the spectral theory of the Koopman operator in dynamical systems and control theory. *54th IEEE Conference on Decision and Control (CDC),* pp. 7034-7041.

Olalla, C., Levya, R., El Aroudi, A., and Queinnec, I. (2009) Robust LQR Control for PWM Converters: An LMI Approach. *IEEE Transactions on Industrial Electronics*, vol. 56, no. 7, pp. 2548–2558.

Rodrigues, C., Kuiava, R. and Ramos, R. (2011). Design of a linear quadratic regulator for nonlinear systems modeled via norm-bounded linear differential inclusions. *IFAC Proceedings Volumes*, 44(1), pp.7352-7357.

Sun, J. *et al.* (2016). Electrochemical Bubbling Transfer of Graphene Using a Polymer Support with Encapsulated Air Gap as Permeation Stopping Layer. *Journal of Nanomaterials,* vol. 2016, p. 7024246.

Tanaka, K. (1996) An Approach to Stability Criteria of Neural-Network Control Systems. *IEEE Transactions on Neural Networks*, vol. 7, no. 3, pp. 629–642.

Xin, H., Zhao, Q., Chen, D., and Li, W. (2018). Roll-to-Roll Mechanical Peeling for Dry Transfer of Chemical Vapor Deposition Graphene. *Journal of Micro and Nano-Manufacturing,* vol. 6, no. 3, p. 031004.

Zhao, Q., Hong, N., Chen, D., Li, W. (2020). Controlling Peeling Front Geometry in a Roll-To-Roll Thin Film Transfer Process. *Manufacturing Science and Engineering Conference*. Cincinnati, OH.

Zhao, Q., Hong, N., Chen, D., Li, W. (2021). Control Oriented Model of a Roll-to-Roll Mechanical Transfer Process for Flexible Electronics Manufacturing. *Dynamic Systems, Measurement, and Control*. To be submitted.

Zhou, H., Qin, W., Yu, Q., Cheng, H., Yu, X., and Wu, H. (2019). Transfer Printing and its Applications in Flexible Electronic Devices. *Nanomaterials (Basel),* vol. 9, no. 2, p. 283.